On-sky Performance of a High Resolution Silicon Immersion Grating Spectrometer

Jian Ge, Scott Powell, Bo Zhao, Sidney Schofield, Frank Varosi, Craig Warner, Jian Liu, Sirinrat Sithajan, Louis Avner, Hali Jakeman, Jakob A. Gittelmacher & William A. Yoder
Department of Astronomy, University of Florida

Matthew Muterspaugh, Michael Williamson & J. Edward Maxwell
Center of Excellence in Information Systems, Tennessee State University

High resolution infrared spectroscopy has been a major challenging task to accomplish in astronomy due to the enormous size and cost of IR spectrographs built with traditional gratings. A silicon immersion grating, due to its over three times high dispersion over a traditional reflective grating, offers a compact and low cost design of new generation IR high resolution spectrographs. Here we report the on-sky performance of the first silicon immersion grating spectrometer, called Florida IR Silicon immersion grating spectromeTer (FIRST), commissioned at the 2-meter Automatic Spectroscopic Telescope (AST) of Fairborn Observatory in Arizona in October 2013. The measured spectral resolution is R=50,000 with a 50 mm diameter spectrograph pupil and a blaze angle of 54.7 degree. The 1.4-1.8 μm wavelength region (the Red channel) is completely covered in a single exposure with a 2kx2k H2RG IR array while the 0.8-1.35 μm region is nearly completely covered by the cross-dispersed echelle mode (the Blue channel) at R=50,000 in a single exposure. The instrument is operated in a high vacuum (about 1 micro torr) and cryogenic temperatures (the bench at 189K and the detector at 87K) and with a precise temperature control. It is primarily used for high precision Doppler measurements (~3 m/s) of low mass M dwarf stars for the identification and characterization of extrasolar planets. A plan for a high cadence and high precision survey of habitable super-Earths around ~150 nearby M dwarfs and a major upgrade with integral field unit low resolution spectroscopy are also introduced.

Key words: High resolution, silicon immersion grating, robotic telescope, Doppler, infrared, exoplanets, spectrograph and M dwarfs.

1. Introduction

One of the most important questions in all of astrophysics is "How common are Earth-like planets?" One way to answer this question with currently available technology is to look where the signal of an Earth-like planet would be strongest—M dwarfs. Low-mass planets in the habitable zones (HZs) of M-dwarfs yield larger and more frequent signals in both radial velocities (RV) and transits, and have a higher probability of transiting than similar objects around Sun-like stars. For this reason, dedicated searches for planets orbiting low-mass stars received strong support from the ExoPlanet Task Force and 2010 Decadal Survey.

Of particular interest are M dwarfs later than M4, where the mass, size, and temperature of the stars begin to rapidly decrease. To date, most exoplanet searches targeting bright M dwarfs have been conducted at visible wavelengths[1,2,3]. Because the later type stars emit most of their light at redder wavelengths, only those earlier than M4 have been well studied. There are only 12 M4 or later type stars with V < 12 north of -30 degrees[4]. For comparison, there are about 300 nearby

Ground-based and Airborne Instrumentation for Astronomy V, edited by
Suzanne K. Ramsay, Ian S. McLean, Hideki Takami, Proc. of SPIE Vol. 9147,
91471A · © 2014 SPIE · CCC code: 0277-786X/14/$18 · doi: 10.1117/12.2057023

stars M4 or later with J<9[5]. Therefore, for the latest types of stars, an observing program must operate where they emit the most light—NIR.

Previous RV searches of early M dwarfs (mass > $0.4M_{\odot}$) have clearly indicated that short-period *giant* planet companions to early M dwarfs are rare[1,2,3]. However, planetary companions to stars at the peak of the stellar mass function and below (mass < $0.4M_{\odot}$) remain essentially unexplored because they are too faint in the visible wavelengths (V~12-14) to be efficiently observed with optical RV spectrographs[3]. These small stars represent perhaps our best opportunity to detect Earth-mass planets, including those orbiting in the Habitable Zone (HZ), given current levels of RV precision[6]. At the same time, these planets will necessarily be in the solar neighborhood, making them amongst the most important targets for future space-based efforts to directly image Earth-like planets and to study their atmospheres.

There is mounting evidence that low mass planets, including the Neptune-mass planets, the super-Earths and Earth-size planets, may be very common in orbit around low-mass stars[7,8]. Analysis by Howard et al. of *Kepler* data indicates that up to 30% of early M dwarfs have super-Earth sized planets with orbital periods less than 50 days. Analysis by Dressing and Charbonneau finds that the occurrence rate of 0.5–4$R_{\oplus}$ planets with orbital periods shorter than 50 days is ~0.90 planets per star. The occurrence rate of Earth-size (0.5–1.4 $R_{\oplus}$) planets is at ~0.51 Earth-size planets per star. Analysis of the HARPS RV data by Bonfils et al. (2013) finds similarly high values for the rate of occurrence of super-Earths orbiting early M dwarfs with periods < 100 days (~35%).

A broad band NIR high-resolution spectrograph is an ideal tool to efficiently search for planets around late M dwarfs because it can capture many stellar absorption lines at the peak of the stellar spectral energy distribution for precision RV measurements. Simulations[9,10] show that the NIR wavelength bands (Y, J, H and K) are the favorite wavelength regions for better Doppler precision for late M dwarfs. However, it has taken major efforts to develop NIR high precision Doppler techniques. Over the past few years, the NIR RV measurement precision has been largely improved from ~100-300 m/s with NIRSPEC on the Keck telescope[11-13] to ~35 m/s with CRIRES on VLT[14]. The current state-of-the-art for NIR RV detection of planets around late M dwarfs has been demonstrated with the VLT's CRIRES with a long-term (~6 months) RV precisions of 5 m/s[15]. The major reason for this large improvement is that a better calibration method (e.g., an ammonia absorption cell), a very high-resolution spectrograph (R=100,000) and careful telluric absorption line modeling and removal were applied in the RV measurements and analysis. However, a lack of dedicated NIR high-resolution spectrographs is the main reason that the NIR Doppler technique is many years behind the highly successful optical Doppler technique in detecting and characterizing exoplanets, essentially leaving the majority of M dwarfs unexplored.

In 2009-2013, we developed a new generation high resolution NIR spectrograph, called Florida IR Silicon immersion grating spectromeTer (FIRST), the first dedicated NIR high-resolution spectrograph for a NIR high Doppler precision M dwarf planet survey with the 2-meter Automatic Spectroscopic Telescope (AST) at Fairborn Observatory in Arizona. The automatic queue nature of the telescope with FIRST enables two key things for the detection of Earth-like planets around M dwarfs with NIR RVs: *better precision and higher cadence*. FIRST was

commissioned at Fairborn in October 2013 and has been tested since to improve its performance before we are ready to launch a pilot survey late in 2014, followed with a full survey of ~150 M dwarfs in 2015-2017. Below we summarize the instrument design, its on-sky performance measurements, remaining technical issues, the planned low-mass planet survey and an upgrade plan with a fiber bundle integral field unit low resolution spectroscopy.

2. The FIRST NIR High-resolution Spectrograph

FIRST is a new generation, fiber-fed, highly stable, cryogenic, NIR high resolution, cross-dispersed echelle spectrograph operated in a vacuum chamber. FIRST adopts a white pupil design, the same as HARPS[16] and TOU (formerly EXPERT-III)[17], which enables a very compact instrument and allows effective management of scattered light. However, FIRST uses VPH gratings as cross-dispersers (Figure 2.1)[6]. FIRST is fed with an 80 μm diameter fiber from the telescope at *f*/4, corresponding to 2.1 arcsec on sky. FIRST implements a reflective Bowen-Walraven Image Slicer[18] to slice the input science beam into two halves and place them in a row to double the spectrograph spectral resolution. It has two channels: a Blue channel with a commercial R4 (76 deg blaze angle) echelle to cover 0.8-1.35 μm at R=50K and a Red channel with a UF made silicon immersion grating (SIG) as the main disperser to simultaneously cover 1.4-1.8 μm at R=50K. The FIRST Blue channel covers 31 spectral orders (orders 46-76, Table 2.1 and also see Figure 2.2) at 0.8-1.35 μm in a single exposure with 95% wavelength coverage while the Red channel completely covers 59 spectral orders (orders 195-253, Table 2.1

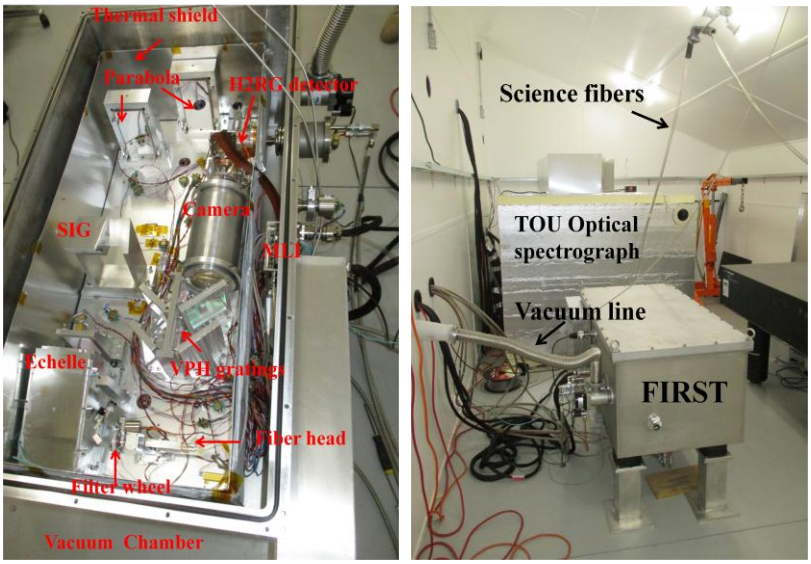

Figure 2.1.(Left). Inside of the FIRST NIR spectrograph. The FIRST bench has 1.0x0.5 meter in dimension. (Right). FIRST, next to the TOU optical high resolution spectrograph, inside an A/C room next to the AST 2m robotic telescope.

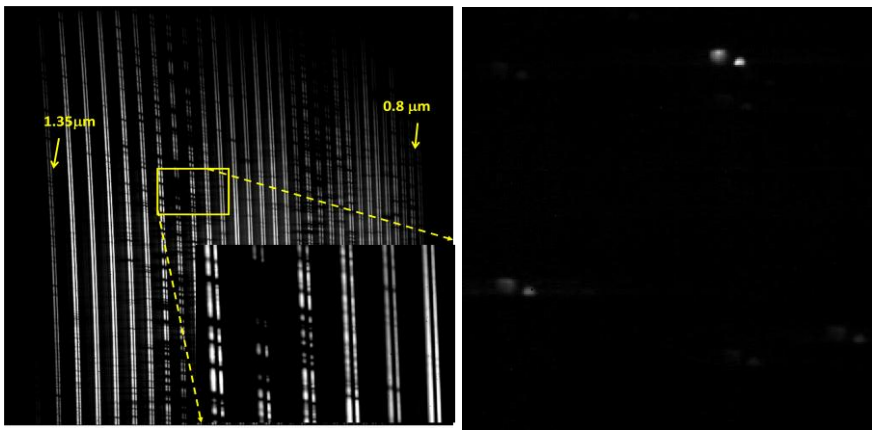

Figure 2.2. (Left). A stellar spectrum of α Ori in 1 min exposure with the FIRST blue channel at R=50K. (Right). ThAr emission line spectrum taken with the FIRST Blue channel. Each emission line has two sliced spectral images, one is well focused while the other is slightly out of focus.

and also see Figure 2.3) at 1.4-1.8 μm in a single exposure. The spectra are recorded with an H2RG 2K×2K array from Teledyne Technologies Inc with 2.57 μm long wavelength cutoff. Two thermal blocking filters plus a PK50 glass plate are installed before the detector to cut off thermal radiation beyond 1.8 μm (Mahadevan 2013, private communications). The detector is controlled by the standard ASIC card. The entire instrument bench (1.0x0.5 meter in dimension) is installed inside a vacuum chamber. The chamber maintains high vacuum at a micro torr level with continuous pumping and an activating cold charcoal-based getter.

A 30-layer MALI thermal shield is mounted around the bench to largely insulate the bench from the chamber thermally. The optical bench is cooled with two cryotigers using standard NF-55 gas and operates at ~189K to reduce the thermal background while the detector is cooled by one cryotiger with PT-13 gas and runs at ~86K to reduce its dark current. Small heaters and Lakeshore temperature sensors are placed on the bench and the detector assembly to allow the bench and detector temperature precisely controlled.

Table 2.1. FIRST instrument parameters

Wavelength region	0.8-1.8 μm
Focal plane	2048x2048 H2RG
Pixel size	18 μm
Detector QE	81% 0.6-1.0 μm 90% 1.0-2.4 μm
Spectral resolution	R=50K at 0.8-1.35 μm (Blue) R=50K at 1.4-1.8 μm (Red)
Dispersion per pixel	0.10Å/pix at 1.25 μm (Blue) 0.11 Å/pix at 1.65 μm (Red)
Sampling	2.4 pixels in the Blue and 2.9 pixels in the Red
Fiber diameter	2.1 arcsec (80 μm)
Spectral orders	46-76 (0.8-1.35 μm) (Blue) 195-253 (1.4-1.8 μm) (Red)
Single exposure coverage	0.52 μm at 0.8-1.35 um (Blue) 0.4 μm at 1.4-1.8 μm (Red)
Design type	White pupil + refractive camera
Collimated beam	50 mm in diameter
Main dispersers	R4, 31.6 l/mm, 76° blaze (Blue) SIG, 16.1 l/mm, 54.74° blaze (Red)
Cross-dispersers (VPH gratings)	240 l/mm 7.0° blaze (Blue) 310 l/mm, 14.0° blaze (Red)
Optical bench	1.04x0.45 meter

FIRST Measured Performance: FIRST was commissioned at the AST 2m telescope at Arizona on Oct. 20-29 2013. We were able to obtain spectra from bright objects, such as α Ori and Vega, with both channels to calibrate its on-sky transmission and demonstrate its science capability as shown in Figure 2.2 and 2.3. The calibration and on-sky measurements show that spectral resolution (FWHMs are about 2.9 pixels and 2.5 pixels for the Red and Blue channels, respectively, Figure 2.4), corresponding to

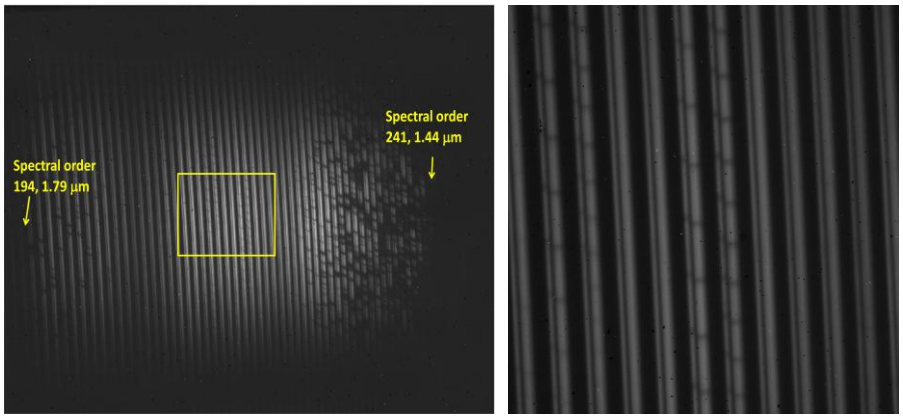

Figure 2.3. (Left). A stellar spectrum of Vega in 5 min exposure with the FIRST SIG channel (or Red channel) at R=50K. The twe close spectra are produced by an image slicer for doubling the spectral resolution. (Right). Zoom-in spectral image of the middle box on the left image. Sharp telluric absorption lines are clearly visible.

R≈50K for both channels. The entire 1.4-1.8 μm wavelength region is completely covered by the Red channel, while about 95% wavelengths between 0.8-1.35 μm are covered by the Blue channel in a single exposure, meeting the design requirements. Due to the extra light path in the image slicer, the sliced image in the Blue channel shows slightly defocus as shown in Figure 2.2. The SIG spectrum of UrNe lamp shows very small level (~0.7%) of ghosts at both sides of the primary emission line as shown in Figure 2.4. This is caused by the small periodic error in the grating photomask and can be further reduced by using a better quality photomask. We have processed sky spectrum taken with FIRST at the observatory and compare it with the synthetic solar spectrum produced from the solar template obtained at the NSO solar telescope. Figure 2.4 also shows part of the reduced sky spectrum at the 1.57 μm region using the IRAF program superimposed with a solar spectrum at the same region. The two spectra match well with each other, indicating that the SIG can produce science quality high resolution spectroscopic data. We did not measure the overall detection efficiency for both the Blue and Red channels as we noticed that the telescope optics plus fiber transmission in the NIR is poor. We are investigating optics in the optical train and trying to identify the major optical components which have contributed to most of photon losses and will make correction in the fall 2014.

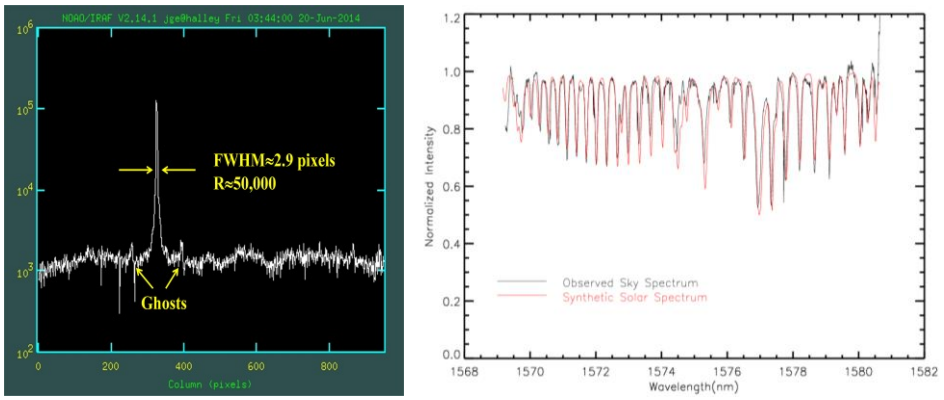

Figure 2.4. (Left). A Neon emission line spectral intensity profile in the logarithmic scale at 1.5604 μm. (Right). A reduced solar spectrum of atmospheric CO_2 band at 1.57-1.58 μm (the spectral order 227) taken and its comparison with an R=50K synthetic telluric spectrum from the solar archival data (National Solar Observatory).

Table 3.1. FIRST instrument transmission budget.

Name	Baseline	Pessim.
Atmosphere		
0.9 μm	0.91	0.91
1.25 um	0.99	0.99
1.55 um	0.98	0.98
Telescope	0.86	0.57
Seeing coupling	0.59	0.53
Fiber+ mode scramb.		
0.9 μm	0.65	0.62
1.25 um	0.67	0.63
1.55 um	0.67 [a]	0.67 [a]
Spectrograph+filters		
0.9 μm	0.24	0.18
1.25 um	0.24	0.18
1.55 um	0.25 [a]	0.25 [a]
Detector		
0.9 μm	0.81 [b]	0.81 [b]
1.25 um	0.90 [b]	0.90 [b]
1.55 um	0.90 [b]	0.90 [b]
Overall efficiency		
0.9 μm	**0.06**	**0.03**
1.25 um	**0.07**	**0.03**
1.55 um	**0.08**	**0.03**

[a] lab measured values, [b]Teledyne measured values

The instrument thermal background is relatively high, e.g., the mean dark current is about 370 ADUs per pixel in a 10 min dark exposure. Figure 2.5 shows the dark current measurements at different exposure time. The relatively high dark current is primarily caused by the thermal radiation of the thermal shield staying at about 206.6K (-66.5°C), which is about 18 degree warmer than the instrument bench (Figure 2.5). The instrument thermal stability is quite good even without turning on the temperature control. Figure 2.5 also shows the bench temperature

measurements over five days. The bench temperature stays within 20 mK (P-V) of the mean temperature at 189.32K (-83.83°C).

3. Remaining Technical Issues and Mitigation Plans

Although FIRST has demonstrated its capability for high resolution NIR spectroscopy, a few major technical issues besides the overall detection efficiency have been identified during the FIRST on-sky testing. These issues must be addressed before the instrument is ready for on-sky RV measurements of nearby bright M dwarfs for the planned planet survey.

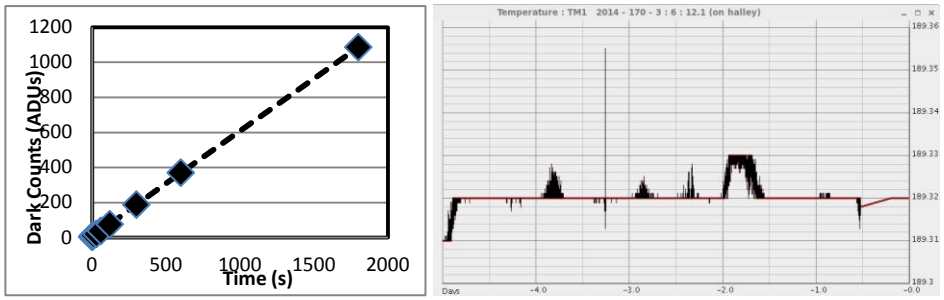

Figure 2.5. (Left). Dark current measurements of the FIRS H2RG detector. (Right). The instrument bench temperature measurements over five days.

1) Large scattered light in the cross-dispersing direction caused by VPH grating cross-dispersers, which is especially severe in the Blue channel (Figure 3.1). This is caused by difficulty in manufacturing the VPH grating with very coarse groove density (240 l/mm for the Blue channel and 310 l/mm for the Red channel). A new grism made of a VPH grating sandwiched with two prisms has been designed and will be manufactured by Kaiser optics to replace current Blue channel VPH grating to increase its throughput to ~90% from current ~60% while substantially reducing the scattered light level in the cross-dispersion direction.
2) Thermal background is still relatively high (~0.6 ADUs/s/pixel), which affects data quality for relatively faint targets. We plan to purchase a third Cryotiger and link the cold head to the thermal shield to reduce its temperature to the same level as the bench to largely reduce the thermal background. This will greatly increase the instrument sensitivity for both high resolution and low resolution IFU spectroscopy.
3) The SIG groove density is two times higher than that necessary for covering the entire 2k×2k H2RG detector with cross-dispersed spectra, leading to quite dense packing of over 50 relatively short spectral orders at 1.4-1.8μm. This SIG was designed to match with a 1k×1k InSb detector when it was developed in 2004-2005. The detector technology has greatly been improved since and the 2k×2k H2RG detector is used in FIRST to leave about half of the detector pixels in the cross-dispersion direction unused for spectrum recording. We plan to develop a new science grade SIG with 32 l/mm and 63.5 degree blaze angle (R2) to increase its free spectral range by a factor of two to take full advantage of the 2k×2k detector resource to cover the entire cross-dispersed spectra

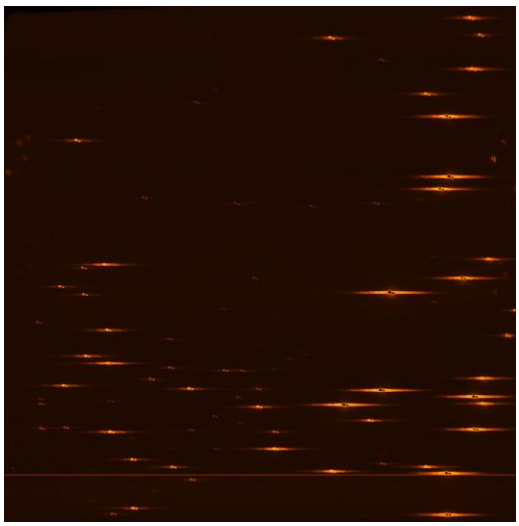

Figure 3.1. ThAr spectrum taken with the FIRST Blue channel. The integrated scattered light level in the cross-dispersion has reached to ~10% level.

while doubling the spectral order separations. The R2 SIG will also increase the FIRST spectral resolution by a factor of 1.4 times.

4. The High Cadence and High Precision Low-mass Planet Survey

Our FIRST M dwarf low mass planet survey will monitor a total of 150 M dwarfs (100 of them are M3.5-M9V and 50 of them are M0-M3.5V dwarfs) in 2015-2017 with the Blue channel (0.8-1.35 μm) which provides slightly better Doppler sensitivity than that provided by the Red channel (the H band) Doppler spectroscopy[10]. We adopt a totally different planet survey strategy than the previous M dwarf survey using HARPS[3]. Instead of surveying over a large number of targets with various RV measurements (from a few RV data points to hundreds of measurements for GJ 581 and GJ 163[19,20]), the FIRST survey will offer a homogeneous high cadence for every survey target, i.e., 100 RV measurements randomly spread over ~300 days. We plan to monitor ~50 new targets each year. The robotic (automatic) nature of the AST telescope at Fairborn Observatory and its flexible queue observation schedule are the key to realizing this homogenous high cadence. This homogeneous high cadence data would provide the best data set for statistical studies of low mass planets around M dwarfs. As illustrated in Figure 4.1, our survey strategy allows for probing most of the parameter space in the planet mass-period distribution of nearby M dwarfs to independently verify characteristics (such as distribution and occurrence rates) of the close-in low mass planet population identified by the *Kepler* mission. Since our survey window covers the HZs of all of the M dwarf survey targets, this survey would also offer an unbiased sampling of HZs to assess habitability of close-in low mass planets around nearby M dwarfs.

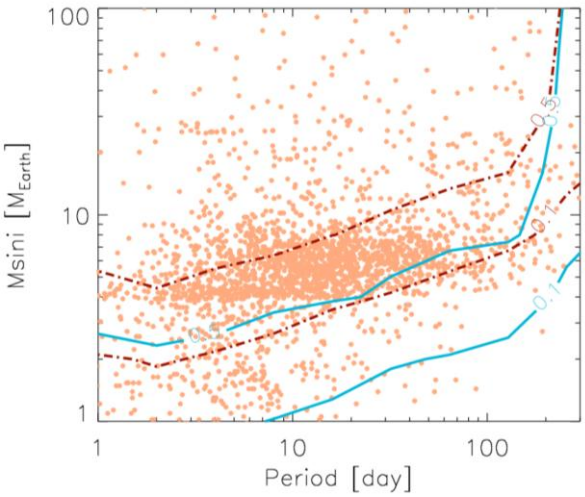

Figure 4.1. The predicted contours (10% and 50%) of the FIRST survey completeness (the blue and red lines represent the optimistic and the pessimistic cases) based on the survey targets, observation strategy, cadence and RV precision. Orange dots are Kepler planet candidates[21]. Masses of *Kepler* planet candidates are derived from the mass-radius relations[22].

4.1. Survey Target Selection & Strategy

We have adopted the following strategy to choose our survey initial targets for this M dwarf survey. We have chosen the brightest M dwarfs in each of the M sub spectral types (M0V to M9V), which does not have known close binaries (within 5 arcsec) and/or reported stellar activities, for the survey observations[23,24] and tried to balance number of survey stars in each sub spectral type (e.g., M0=13 stars, M1=12 stars, M2=13 stars, M3=12 stars, M4=30 stars, M5=29 stars, M6=16 stars, M7=13 stars, M8/9=12 stars). We plan to observe these initial targets ~5 times with FIRST. After ~5 RV measurements for each target, we reject those targets with significant RV jitters (e.g., ≥3 m/s) or spectroscopic binary RV signals and replace it with the next brightest target in the same spectral sub type catagory and continue the same vetting process until the target passes the initial vetting process. The final vetted survey targets will only include those M dwarfs without significant level of stellar activities and close-in spectroscopic binaries.

Figure 4.2 shows distributions of our initial survey targets, including magnitude, effective temperature and mass.

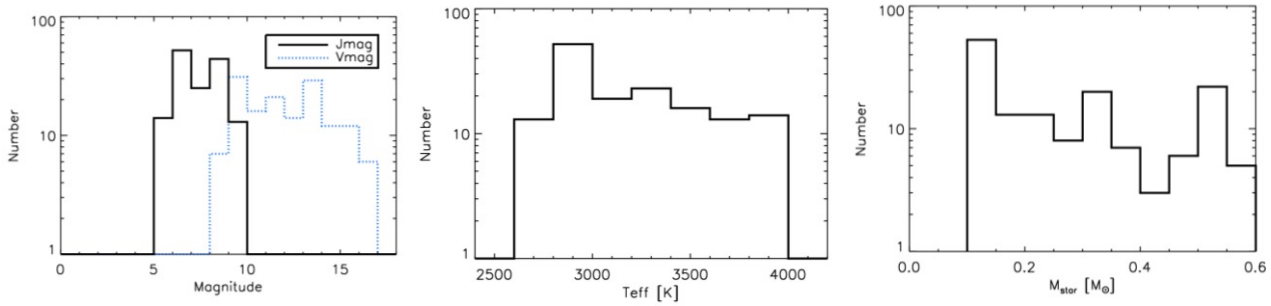

Figure 4.2. (Left). J and V magnitude distribution of selected M dwarfs for the FIRST low-mass planet survey. (Middle). T_{eff} distribution of the selected survey targets. (Right). Stellar mass distribution of the selected survey targets.

4.2. Doppler Sensitivity and Predicted Planet Yield Doppler sensitivity: We use high-resolution synthetic stellar spectra, generated by the PHOENIX code[25,26], to calculate photon-limited RV uncertainties with FIRST. The FIRST instrument parameters listed in Table 2.1 were used in spectral synthesis. Figure 4.3 shows photon noise limited RV measurement errors for different effective temperature and rotational velocities with the Blue channel. To predict the real RV measurement errors, we included measurement uncertainties from instrument RV calibration, contamination of telluric lines (absorption lines and OH emission lines), fiber illumination variations caused by the telescope guiding, tracking and seeing, instrument thermal drift, and data pipeline. In the NIR region, telluric lines (especially absorption lines) are nearly everywhere. Modeling and removal of telluric contamination becomes a critical part of data processing to reach close to the photon noise limit[13,10,27]. We calculated additional RV errors caused by masking out all of the telluric absorption lines at the 2% depth level and removing OH emission lines at the above 1% of the peak intensity level. We keep the RV uncertainty caused by the fiber illumination profile changes to within 0.5 m/s by scrambling fiber modes with a 3-lens optical mode scrambler[28,29] with a measured gain of ~3000 in FIRST. We budget the RV measurement error caused by the thermal drift to within 0.5 m/s by controlling the instrument long-term thermal stability to within ~2 mK (rms). Therefore, the illumination error and thermal drift error can be negligible compared to telluric line induced errors. Given many uncertainties in our RV extraction codes, we budget that the data pipeline can deliver 1.5 times the photon error. We use the following error budgets in simulating our survey sensitivity and planet yields,

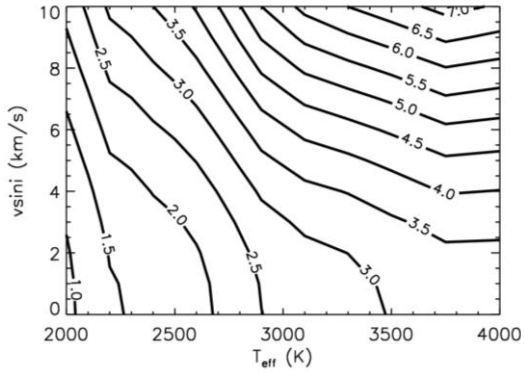

Figure 4.3. Photon noise limiting RV measurement errors for M dwarfs with different effective temperatures (spectral type) and stellar rotational velocities with S/N=150 per pixel at 1.25 μm.

- Optimistic case: 1.5*photon noise+ 0.5 m/s (calibration error)+2.0 m/s (telluric)
- Pessimistic case: 3.0*photon noise+ 0.5 m/s (calibration error)+2.0 m/s (telluric)+3.0 m/s (long term systematic error).

Therefore, our optimistic case represents possible RV performance for a survey star without significant activity induced RV jitters and instrument systematic errors other than the calibration error, while the pessimistic case represents a possible case including significant long-term systematic errors, such as stellar jitters and other systematic errors. Figure 4.4 shows predicted RV precision of our survey targets with 30 min exposure (assuming 4% total detection efficiency) following the above measurement error consideration.

Predicted planet yield: We conducted survey simulations to derive survey sensitivity and completeness. We applied the survey strategy (100 RV measurements randomly distributed over 300 days) and real observation conditions (night time window and also average weather conditions at Fairborn Observatory) in the simulations. RV performances for both optimistic and pessimistic cases are used in the simulations. As mentioned in section 4.1, we will minimize the impact of stellar jitters on our RV performance by passing our potential survey targets with unknown jitter levels through a reconnaissance pilot survey and rejecting those with jitter level above 3 m/s. Figure 4.1 shows survey detection sensitivity and completeness level from both optimistic and pessimistic cases. It is quite interesting to see that our proposed high cadence survey can detect nearly all of the known low-mass planet candidates identified by *Kepler* if we can reach high RV precision (~3 m/s) for the majority of our survey targets with our FIRST. Even under the pessimistic case, we can still detect a majority (~80%) of the *Kepler* super-Earth population thanks to our high cadence strategy. The survey sensitivity with FIRST is comparable to TOU in the optical due to the smaller mass of the M dwarfs than the earlier spectral type dwarfs observed by TOU and brighter NIR flux than the optical flux measured by TOU although it delivers 3 times worse RV performance[30].

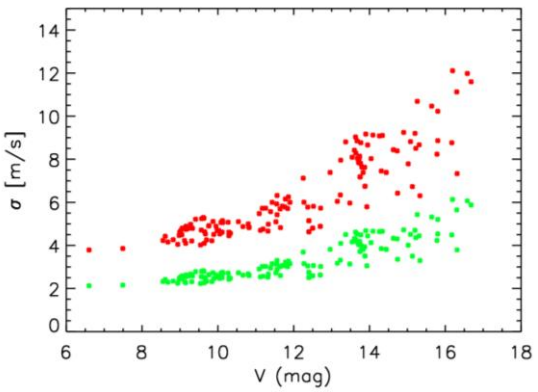

Figure 4.4. Predicted RV measurement precision of our survey targets in the optimistic case (green dots) and pessimistic case (red dots).

Table 4.1 lists our predicted planet yields based on the optimistic and pessimistic cases. Our final yield is likely to fall between. The following planet occurrence rate within 300 days are used in the yield calculations: Earth-size planets (1-1.25$R_\oplus$), 16.1%; super-Earths (1.25-2 $R_\oplus$), 32.9%; and small Neptunes (2-4 $R_\oplus$), 30.9%[31]. The mass for each planet is determined by empirical formula (equations (1), (2) and (3)) in Weiss & Marcy[22]. We used the planet occurrence rates for 0.8-245 days as our rates for the above calculations. For those which do not have the rates in this period range, we extrapolated the rates from those derived from the smaller period ranges (such as super-Earths and Earths) in Table 3 of Fressin et al's paper[31]. The large systematic measurement errors of 3 m/s applied to all of the survey stars in the pessimistic case has significantly reduced our detection sensitivity for Earth-size planets and also super-Earths, but has relatively small impact in the detection of close-in small Neptunes. About half of the super-Earths around M dwarfs in the optimistic and pessimistic cases,

Table 4.1. Predicted planet yields from the high cadence survey

	Earth-size	Super-Earths	Small Neptunes
Optimistic	4	21	30
Pessimistic	1	9	20

respectively) will be in their HZs (33% without cloud coverage and 73% with full cloud coverage)[6] and one of them may be a transiting planet. Our optimistic detections would possibly provide sensitive measurements of planet occurrence rates for these three types of low mass planets. *This sample would also offer a large collection of HZ rocky planets around nearby M dwarfs using ground-based telescopes.* Our pessimistic detections would possibly offer sensitive measurements of planet occurrence rates for super-Earths and small Neptunes. In either case, the overall planet sample will substantially increase the power for statistical study of planet occurrence and properties and constraints on planet formation models and physical conditions around low mass stars.

5. Major Upgrade

We are working on implementing a fast response fiber-fed IFU 3-D imaging spectroscopy mode in FIRST to capture high-*z* Gamma Ray Bursts (GRBs) shortly after the burst triggers. The IFU, made of a circular shape fiber bundle with 25 80 μm core diameter fibers (2.1 arcsec on sky at *f*/4 for each fiber) and relay optics, can simultaneously capture spectra of all objects within ~10 arcsec FOV. By inserting an IFU optics, FIRST can offer an R=900 spectroscopy at 0.8-1.35 μm or R=2000 at 1.4-1.8 μm in a single exposure. Figure 5.1 shows the optical layout of the IFU mode in FIRST. The telescope beam, bypassing the first parabola, the high dispersing element and the spectral mirror, is fed directly into the second parabola of FIRST and forms a collimated beam to pass through one of the VPH gratings to produce low resolution IR spectra. The fiber bundle FOV, much larger than the GRB coordinate uncertainty of ~3-5 arcsec provided by the Swift X-Ray Telescope (XRT), allows a prompt capture of a GRB NIR spectrum in ~2 min telescope slewing time to obtain high signal-to-noise (S/N) data without the usual time delay caused by the object acquisition and target identification of the typical long-slit spectrograph at other observatories. The NIR wavelength coverage (0.8-1.8 μm) is ideal for identifying GRBs in the redshift range z~5.5-13.5 through the Lyman alpha break signature (i.e. the Gunn-Petersen trough). We expect to complete the IFU upgrade by the end of this fall.

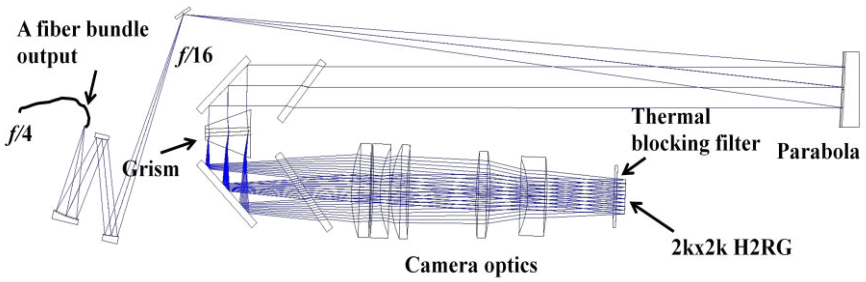

Figure 5.1. The optical layout for the IFU medium resolution spectroscopy mode. By choosing a "blue" filter (0.8-1.35 μm) or a "red" filter (1.4-1.8 μm), the collimated beam passes either the "blue" VPH grating or the "red" VPH grating to get dispersed and form 25 low resolution spectra on the 2kx2k H2RG detector.

6. Conclusions and Future Work

The telescope engineering data taken with the commissioned FIRST NIR spectrograph show that the instrument has delivered its required spectral resolution of R=50,000 in both the Blue (0.8-1.35 μm) and Red channels (1.4-1.8 μm). Several major technical areas (such as the telescope and fiber transmission in the NIR, scattered light from the cross-dispersers and the instrument thermal background) have been identified and efforts are being made to improve the telescope and fiber NIR transmission, reduce scattered light from the cross-dispersers and thermal background. After these major issues are addressed this fall, the instrument will be tested with

RV reference stars to characterize its RV measurement performance. Once RV performance meets survey requirements, we will launch a pilot survey of 20 M dwarfs to characterize its science capability before launching the full survey in 2015.

Acknowledgement: This work has been supported by DoD Cooperative Agreement W911NF-09-2-0017, NSF AST-0451408, NASA NAG5-11427, NASA NNX14AI93G, NSF-PAARE grant 1059158, state of Tennessee through its Centers of Excellence program and the University of Florida.

REFERENCES

1) Endl, M. et al. "Exploring the Frequency of Close-in Jovian Planets around M Dwarfs," ApJ, 649, 436 (2006).
2) Johnson, J. et al. "A New Planet around an M Dwarf: Revealing a Correlation between Exoplanets and Stellar Mass," ApJ, 670, 833 (2007)
3) Bonfils, X. et al. "The HARPS search for southern extra-solar planets. XXXI. The M-dwarf sample," 549, 109 (2013a).
4) Reid, I. N. & Gizis, J. "Low-Mass Binaries and the Stellar Luminosity Function," AJ, 113, 2246 (1997)
5) Lepine, S. & Shara, M. "A Catalog of Northern Stars with Annual Proper Motions Larger than 0.15" (LSPM-NORTH Catalog)," AJ, 129, 1483 (2005)
6) Ge, J. et al. "High Resolution Florida IR Silicon Immersion Grating Spectrometer and an M Dwarf Planet Survey," Proc. SPIE, 8446E, 3OG (2012a)
7) Howard, A. et al., "Planet Occurrence within 0.25 AU of Solar-type Stars from Kepler," 201, 15 (2012).
8) Dressing, C. D. & Charbonneau, D. "The Occurrence Rate of Small Planets around Small Stars," ApJ, 767, 95 (2013).
9) Reiners, A., Bean, J., Huber, K., Dreizler, S., Seifahrt, A., & Czesla, S. "Detecting Planets Around Very Low Mass Stars with the Radial Velocity Method," ApJ, 710, 432 (2010)
10) Wang, J. & Ge, J., "How Close Are We To Detecting Earth-like Planets in the Habitable Zone Using the Radial Velocity Technique?" arXiv:1107.4720 (2011).
11) Martín, E. et al. "A Multiwavelength Radial Velocity Search for Planets around the Brown Dwarf LP 944-20," ApJ, 644, 75 (2006)
12) Zapatero Osorio, M. et al. "Infrared radial velocities of vB 10," A&A, 505, 5 (2009).
13) Blake, C.H. et al. "The NIRSPEC Ultracool Dwarf Radial Velocity Survey," ApJ, 723, 684 (2010).
14) Huelamo, N. et al. "TW ;Hydrae: evidence of stellar spots instead of a Hot Jupiter," A&A, 489, L9 (2008)
15) Bean, J. et al. "The CRIRES Search for Planets Around the Lowest-mass Stars. I. High-precision Near-infrared Radial Velocities with an Ammonia Gas Cell," ApJ, 713, 410 (2010)
16) Pepe, F., et al. " HARPS: ESO's coming planet searcher. Chasing exoplanets with the La Silla 3.6-m telescope," The Messenger (ISSN 0722-6691), No. 110, p. 9 – 14 (2002).
17) Ge, J. et al. "Design and Performance of a New Generation, Compact, Low Cost, Very High Doppler Precision and Resolution Optical Spectrograph," Proc. SPIE, 8446E, 8RG (2012b).
18) Bowen, I.S. "The Image-Slicer a Device for Reducing Loss of Light at Slit of Stellar Spectrograph," ApJ, 84, 113 (1938).

19) Mayor, M. et al. “The HARPS search for southern extra-solar planets. XIII. A planetary system with 3 super-Earths (4.2, 6.9, and 9.2 $M_{\oplus}$),” A&A, 493, 639 (2009)
20) Bonfils et al. “The HARPS search for southern extra-solar planets. XXXIV. A planetary system around the nearby M dwarf GJ 163, with a super-Earth possibly in the habitable zone,” A&A, 556, 110 (2013b).
21) Batalha, N. et al. "Planetary Candidates Observed by Kepler. III. Analysis of the First 16 Months of Data," ApJS, 204, 24 (2013).
22) Weiss, L., & Marcy, G. W., "The Mass-Radius Relation for 65 Exoplanets Smaller than 4 Earth Radii," ApJ, 783, 6 (2014).
23) Lepine, S. et al. “A Spectroscopic Catalog of the Brightest (J < 9) M Dwarfs in the Northern Sky,” AJ, 145, 102 (2013).
24) Lepine, S. & Gaidos, E. “The northern census of M dwarfs within 100 pc, and its potential for exoplanet surveys,” AN, 334, 176 (2013).
25) Hauschildt, P. H., Allard, F., & Baron, E. “The NextGen Model Atmosphere Grid for 3000<=T_{eff}<=10,000 K,” ApJ, 512, 377 (1999).
26) Allard, F. et al. “The Limiting Effects of Dust in Brown Dwarf Model Atmospheres,” ApJ, 556, 357 (2001).
27) Wang, J., Ge, J., Peng, J., & Zhao, B. “Fundamental Performance of a Dispersed Fixed Delay Interferometer in Searching for Planets around M Dwarfs,” ApJ , 738, 132 (2011)
28) Pepe, F. et al. “HARPS: a new high-resolution spectrograph for the search of extrasolar planets,” Proc. SPIE, 4008, 582 (2000)
29) Barnes, S. I. & MacQueen, P.J., “A high-efficiency fibre double-scrambler prototype,” Proc. SPIE, 7735, 204 (2010).
30) Ge, J. et al. “A Robotic, Compact and Extremely High Resolution Optical Spectrograph for a Close-in Super-Earth Survey,” Proc. SPIE, 9147, 308 (2014)
31) Fressin, F. et al. "The False Positive Rate of Kepler and the Occurrence of Planets," ApJ, 766, 81(2013).